FRACTAL BASED CANCER MODELLING

Authors: MILAN STEHLÍK
– Institute of Statistics,
University of Valparaíso, Chile
Department of Applied Statistics,
Johannes Kepler University Linz, Austria
mlnstehlik@gmail.com

PHILIPP HERMANN
– Department of Applied Statistics,
Johannes Kepler University Linz, Austria
philipp.hermann@jku.at

ORIETTA NICOLIS
– Institute of Statistics,
University of Valparaiso, Chile
orietta.nicolis@uv.cl

Abstract:

• Fractal hypothesis is both challenging and technical issue of mammary cancer. We conduct a simple discrimination on the basis of box-counting dimension. Moreover, we discuss on statistical distributions of fractal dimensions for both mammary cancer and mastopathy. Thereby, we detect significant differences in the underlying distribution between the two groups. A multifractal analysis on the basis of a wavelet based approach has been conducted. Discussion on alternative cancer therapy and cancer prevention is provided.

1.   INTRODUCTION

When we consider fractal based cancer diagnostic, many times a statistical procedure to assess the fractal dimension is needed. We shall look for some analytical tools to discriminate between cancer and healthy ranges of fractal dimensions of tissues (see [3, 19]). Fractal dimension may also help for early diagnosis of breast cancer, which is the key for breast cancer survival. Breast cancer, hereafter described as mammary cancer, is the most common cancer in women. The algebraic and topologic properties of cancer growth are available via appropriate set structure, e.g. bornology (see [20, 21]) or topology (see [28]). Here we illustrate some issues on discrimination between mammary cancer (mamca) and mastopathic (masto) tissues, which is follow-up of study of [13]. The data contains 391 histological images of mammary ($n = 192$) and mastopathic ($n = 199$) tissue, which were used to compute the box-counting dimension by means of ImageJ software [1]. We refer to [12] or [13] for more details how the fractal dimension was obtained. A modelling procedure for mammary cancer and mastopathy on the basis of randomized fractals has been introduced in [12], showing that this flexible model can reconstruct the development of the tissue of both, cancer and mastopathy. This approach allows to measure the fractal dimension with the aid of box-counting dimension, in order to observe the development of the tissue over time as well as to discriminate between these two groups.

Mammogram or sonogram examinations have been used as a first step in cases of breast cancer suspicion. Since biopsy, which is an invasive surgical operation imposing psychological and physiological stress for patients, has to be used to confirm the disease to date, other diagnostic tools with accurate diagnostic rates are of interest to be developed. Recently, computer aided diagnosis systems (CAD) are frequently investigated by researchers, see [4] among others, however, we discriminate between mastopathy and cancer on the basis of statistical differences (e.g. in terms of underlying distributions) in the fractal dimension of the two groups.

2.   SIMPLE DISCRIMINATION BETWEEN MASTOPATHY AND MAMMARY CANCER BASED ON THE BOX-COUNTING DIMENSION

We consider boxplots in Figure 1 in order to have a graphical comparison between the two groups. Therein, the box-counting dimensions seem to be on average lower for mammary cancer tissue in addition that some candidates for outliers are apparent in the lower boundaries.
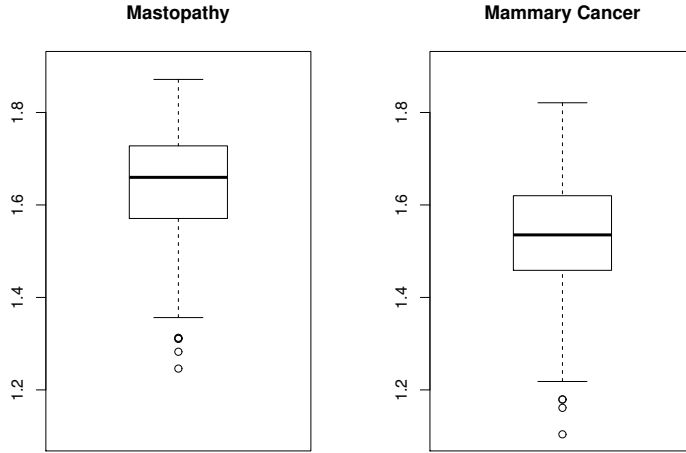
Figure 1: Boxplot of the groups mastopathy (left) and mammary cancer (right).

If we will follow the simple concept that higher dimension is more risky, the issue is that we will arrive with this dataset to some sort of contradiction. When we make a simple clustering based on ordering the box-counting dimension and decide to tell that more risky tissue has a box-counting dimension bigger than the median (1.5972) and non-risky tissue is below, then we only classified 135 of mamca and 60 of masto below. Recall that 199 observations contain the characteristic mastopathy and 192 observations mammary cancer. Even using the arithmetic mean of 1.587391 decreases the number of classified tissues to 128 for mamca and 56 for masto. Based on this simple example we can conclude that we need a more sophisticated procedure based on the box-counting dimension to discriminate between the two groups and we should take more detailed characteristics of the tissue into account. In extremal case there is no possibility to develop automatic clustering based on box-counting dimension, which could avoid histological expert examination.

Figure 2 indicates that using the only single box-counting dimension establishes inverse problems, which are ill posed. Loosely saying we need a continuous dimension spectrum, e.g. multi-fractal dimension spectra. It has already been used in breast cancer discrimination by [6, 10, 22]. A multifractal system is a generalization of a fractal system in which a single exponent (the fractal dimension) is not enough to describe its dynamics; instead, a continuous spectrum of exponents (the so-called singularity spectrum) is needed. This also relates to Tweedie exponential dispersion models, which, as a special case, contain both normal and gamma distributions. This is further justification for these two simple distributional families: in the case of our empirical data we have found a strong deviation from normality for mastopathy, and therefore we used gamma $G(\alpha, \beta)$ and Weibull $W(k, \lambda)$ distribution. In contrast to that mammary cancer data is also tested for normal distribution in the following.

The distribution of the ordered observations of the different groups is highlighted in Figure 2. Apparently, mammary cancer tissue have on average lower dimensions (dashed line) compared to mastopathological tissue (solid line). These conclusions were already recognizable due to the comparison of the mean as well as the interquartile-distance within the boxplots.
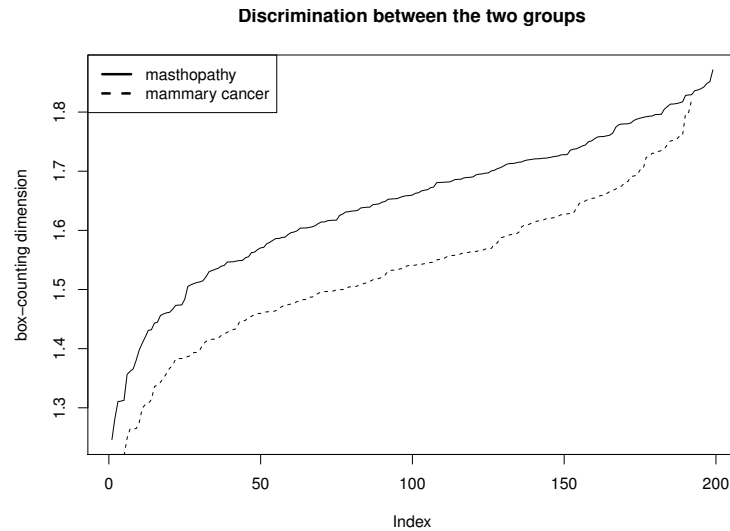

Figure 2: Plot of the dimensions discriminated between the groups mastopathy and mammary cancer.

3. TESTING FOR DISTRIBUTIONS OF THE GROUPS

Separating the data and testing for distributional fit of the groups may lead to further information on group discrimination. Therefore, maximum likelihood procedures have been conducted in order to estimate fitting parameters for gamma and Weibull distribution for fractal dimension of the mastopathy. Estimation for gamma distribution yields a shape equal to 162.58 and scale equal to 98.85, which results in a p-value of 0.15 by usage of Kolmogorov–Smirnov-test (KS-test). For Weibull distribution the two distribution forming parameters were estimated as 16.20 and 1.70. Testing with those parameters gives a p-value of 0.96. Fitting the distributions with estimated parameters in addition to the histogram is plotted on the left part of Figure 3. A better fit of the mammary cancer data with normal distribution has been seen in previous calculations. ML-estimations are computed in order to continue the testing procedure with gamma ($\hat{\alpha} = 129.50$ and $\hat{\beta} = 84.76$ results in $p = 0.43$) and Weibull ($\hat{k} = 13.23$ and $\hat{\lambda} = 1.59$ gives $p = 0.20$) distributions. In addition to that mean (1.53) and variance (0.017) are computed to fit normal distribution ($p = 0.66$). These p-values show that

gamma, Weibull, and normal distribution may not be rejected to fit mammary cancer box-counting dimensions. The right plot of Figure 3 shows the fit for the fractal dimension of mammary cancer data with the parameter estimates given above. Therein, gamma distribution is presented as solid line, Weibull distribution as dotted line and normal distribution is visualized with a dash-dotted line.
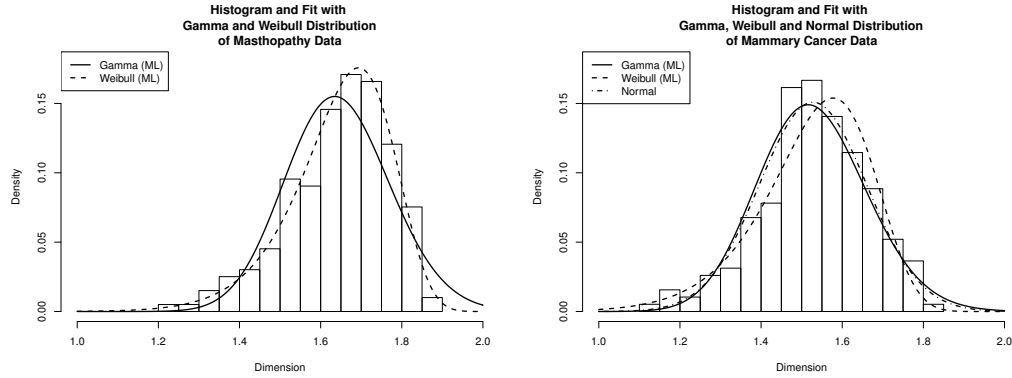

Figure 3: Fit of mastopathy (left) and mammary cancer (right) groups separately.

Table 1 provides the shape and scale parameters for both gamma and Weibull for the complete data as well as both groups separately. Note that parameters for normal distribution are not provided due to lack of comparability, since only for mammary cancer data this distribution was not rejected.

Table 1: Computation of *p*-values for gamma and Weibull distribution with shape and scale parameter for both, complete data and separated by groups mastopathy and mammary cancer.

Distribution	Group	shape	scale	*p*-value
Gamma	All	120.84	76.12	0.22
	Masto	162.58	98.85	0.15
	Mamca	129.50	84.76	0.43
Weibull	All	13.25	1.65	0.39
	Masto	16.20	1.7	0.96
	Mamca	13.23	1.59	0.20

Note that for the total data we received estimator of shape estimator 120.84 and a scale estimator of 76.12 for gamma distribution. KS-test of this set of parameters results in 0.22. Moreover, ML estimation for Weibull distribution gives the estimators 13.25 and 1.65 with a corresponding *p*-value of 0.39. Therefore,

one can see that discriminating between the groups yields differences in terms of underlying distribution parameters. Adjusting the data for outliers results in negligible differences in the estimates.

In the following we will apply that the sum of squared independent standard normal distributed random variables follows Chi-Squared distribution. We will assume:

- The differences between the curves are standard normal distributed. Therefore, Shapiro–Wilk-test can be used. On the given dataset it results in a rejection of the null-hypothesis of standard normal distribution. Hence, there is another possibility to justify the condition in order that usage of Chi-Squared distribution is allowed.
- The squared differences are Chi-Square distributed with one degree of freedom.

Computing the sum of the squared differences delivers a value equal to 5.38. A Chi-Square-test was accomplished to test whether we can distinguish between two groups within the data. The p-value of the distribution function of the Chi-Squared distribution with 199 degrees of freedom is approximately one. This p-value is another proof that the two groups are different. Furthermore, we made a standardization (by subtracting the mean and dividing by the standard error) of the previously calculated differences. The distribution function at the sum of standardized squared differences of 198 and 199 degrees of freedom is 0.49331. Hence, this p-value does not yield enough support to reject the null hypothesis of differences between the groups. However, the property of the data (only positive values) as well as high flexibility of gamma distribution leads us to hypothesis for gamma distribution. We simulated in order to maximize p-values with changes in shape and scale parameters of gamma distribution. By reducing the shape parameter and in contrast to that increasing the rate (reducing the scale parameter), Table 2 shows a convergence to higher p-values.

Table 2:   Simulation of p-values with given shape and scale parameter.

shape	scale	p-value
0.45491680	$\frac{1}{0.45729929}$	$8.354 \cdot 10^{-5}$
0.48	$\frac{1}{0.4573}$	$3.7 \cdot 10^{-12}$
0.44	$\frac{1}{0.4673}$	$1.65 \cdot 10^{-11}$
0.425	$\frac{1}{0.48}$	$1 \cdot 10^{-9}$
0.42	$\frac{1}{0.48}$	0.0049
0.425	$\frac{1}{0.48}$	0.0449
0.43	$\frac{1}{0.48}$	0.0097
0.42	$\frac{1}{0.485}$	0.1272
0.415	$\frac{1}{0.485}$	0.0996

We can see with the aid of KS-test that we will find a rather good fit for specific values of the parameters. Thereby, the shape parameter of 0.415 and a scale parameter of 1/0.485 delivered an accurate p-value of 0.0996. The test with a shape parameter of 0.42 delivered an even better p-value of 0.1272. Therefore, it can be assumed that the standardized differences are gamma distributed with a shape parameter lying in between the range [0.415, 0.42] and the scale parameter close to 2.06 ($\frac{1}{0.485}$). Therefore, we compare the standardized differences with generated random variables of a gamma distribution, with a shape parameter of 0.415 and a scale parameter of 2.062 in Figure 4.
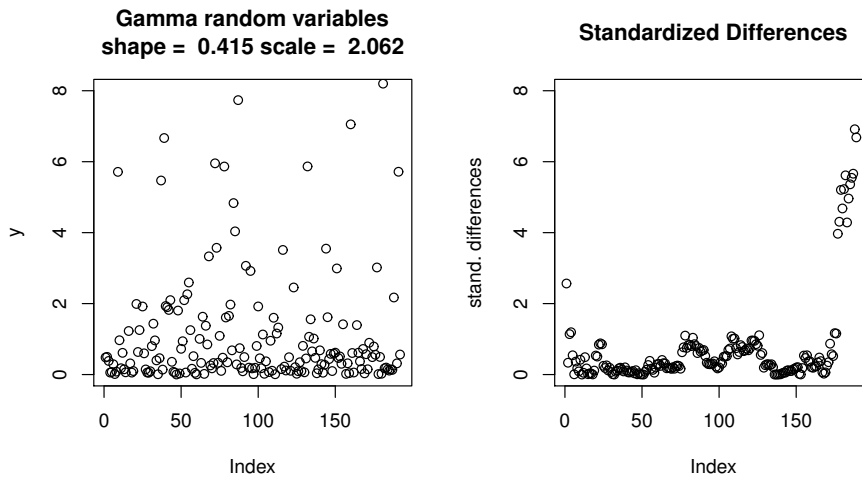

Figure 4:   Comparison of standardized differences with
random variables of a gamma distribution.

Shapiro–Wilk tests deliver a p-value for mammary cancer tissue of 0.0452 and a value smaller than 0.001 was obtained for mastopathic tissue. Hence, for a significance level of 95% both p-values are too small to state that the box-counting dimension of mammary cancer tissue or mathopathic tissue is normal distributed. QQ-Plots in Figure 5 are another indication, that mastopathy is not normal distributed, but normal distribution of the dimensions of mammary cancer should not be rejected without further analysis. Indeed, the lower quantiles differ significantly from the comparative line in the range of -3 to about -1.5 of the theoretical quantiles. Therefore, outlier detection for mammary cancer data with usage of box-plot rule has been performed. These computations are performed with $q_{0.25} - 1.5 \cdot IQR$ and $q_{0.75} + 1.5 \cdot IQR$, where IQR is the interquantile range as $q_{0.75} - q_{0.25}$ and q_{α} is the α-quantile. Four candidates for outliers from the lower end of the data were obtained and removed in order to yield useful information on the distributional behavior of mammary cancer tissue. The according p-value has significantly increased up to 0.5716 and therefore, it can be assumed that the modified data is normal distributed. Another indication for normality of

this group are histogram and QQ-Plot of the modified data in the second row of Figure 5. Both of the plots suggest that the modified box counting dimension of mammary cancer tissue is normal distributed.
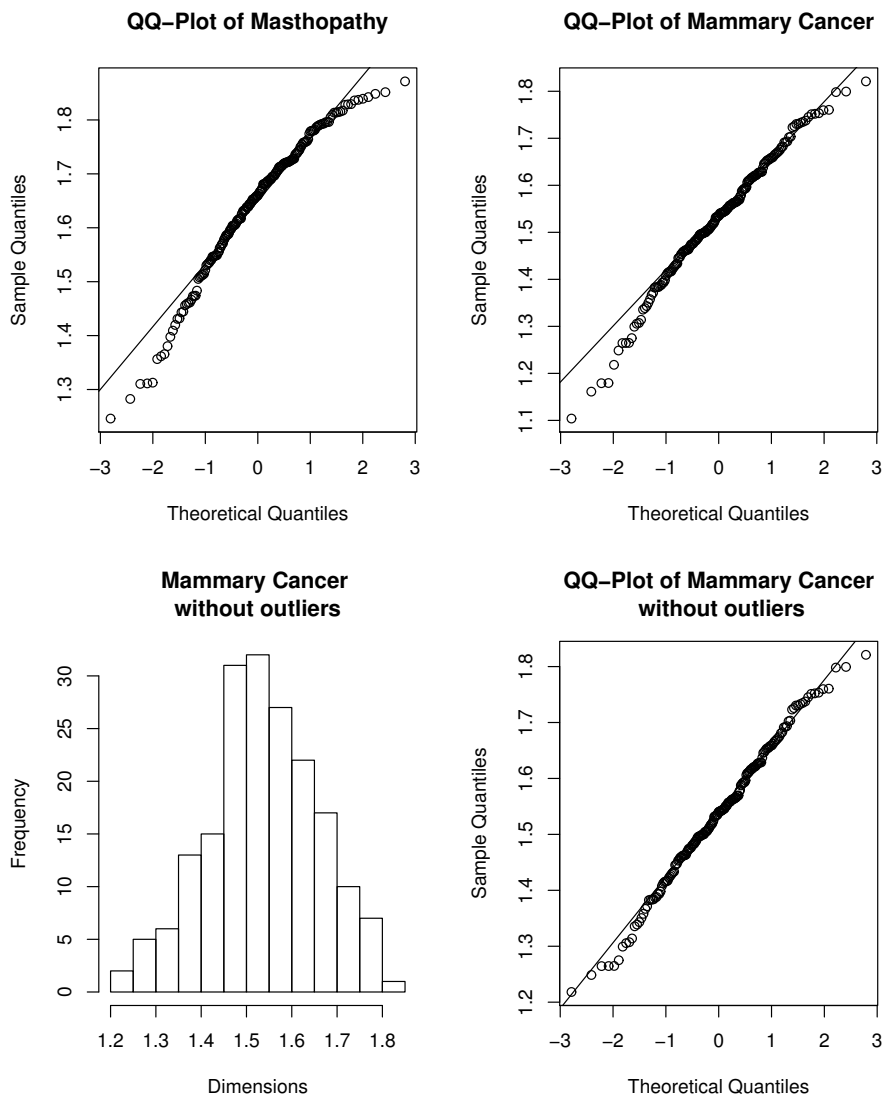

Figure 5: Top row: QQ-Plot of the groups mastopathy (left) and mammary cancer (right). Bottom row: Histogram and QQ-Plot of mammary cancer data without outliers ($n = 188$).

Robust normality testing procedures have been applied to both groups. Therefore, data has been truncated in the lower boundaries, such that only tissue higher than threshold ε has been taken into account. Shapiro–Wilk tests have been used to compute p-values for the fit of normal distribution. The development of p-values can be found in Figure 6, where especially modified box-counting

dimensions of mammary cancer tissue can be seen as normally distributed in contrast to mastopathic tissue box-counting dimensions. This test approach unfolds the different behaviour of the box-counting dimension with respect to normality.
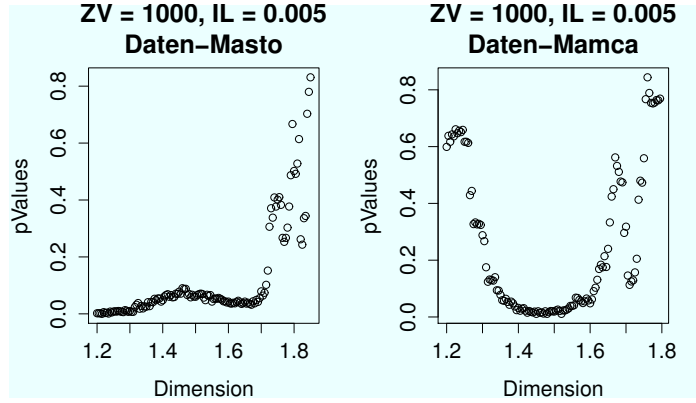

Figure 6:   Test for normal distribution with truncated data for both groups.

Therefore, truncation of the data from the lower boundaries reveals mammary cancer box-counting dimension is more robust with respect to normality than mastopathic tissue.

4.   MULTIFRACTAL ANALYSIS OF MAMMOGRAPHY: A WAVELET BASED APPROACH

Multifractal analysis is concerned with describing the local singular behavior of measures or functions in a Geometrical and Statistical fashion. It was first introduced by Mandelbrot in the context of turbulence (see [17, 18]) even if the term "multifractal", was successively proposed by [9].

Multifractal structures have been found in various contexts. Most prominently in studies of turbulence, stock market exchange rates, geophysics and recently also in traffic, introducing fruitful and novel aspects to the mentioned fields. The basic concept of multifractal analysis is to assess fractal dimensions of self-similar structures with varying regularities and to produce the distribution of indices of regularity, which constitutes the multifractal spectrum (MFS). The multifractal formalism relates the MFS to the partition function measuring high-order dependencies in the data. In the following we will describe the wavelet-based multifractal spectrum (WMFS) proposed by [11, 23, 24] and we will apply it to a sample of mammographic images. The advantages of using the wavelet-based MFS are availability of fast algorithms for wavelet transform, the

locality of wavelet representations in both time and scale, and intrinsic dyadic self-similarity of basis functions. The multifractal formalism is based on the concepts of the partition function which can be defined in terms of wavelet coefficients as

$$(4.1) \qquad T(q) = \lim_{j \to -\infty} \log_2 E|d_{j,k}|^q \,,$$

where $d_{j,k}$ is the wavelet coefficient at level j and location k, and q is the order of moments. We emphasize that q is a real number within a certain range covering the negative numbers as well [11]. Even though (4.1) is very informative, the singularity measure is not explicit. It was proposed in [11] that the local singularity strength could be measured in terms of wavelet coefficients as:

$$(4.2) \qquad \alpha(t) = \lim_{k2^j \to t} \frac{1}{j} \log_2 |d_{j,k}| \,,$$

where $d_{j,k}$ is the normalized wavelet coefficient at scale j and location k. The local singularity strength measure (4.2) converges to the local Hölder index of the process at time t. Small values of $\alpha(t)$ reflect more irregular behavior at time t. Any inhomogeneous process has a collection of local singularity strength measures and their distribution $f(\alpha)$ forms the MFS. A useful tool to estimate the MFS is through the Legendre as follows

$$(4.3) \qquad f_L(\alpha) = \inf_q \big\{ q\alpha - T(q) \big\} \,.$$

It can be shown that $f_L(\alpha)$ converges to the true MFS by using the theory of large deviations [8]. If we rearrange (4.1), it becomes

$$(4.4) \qquad E|d_{j,k}|^q \sim 2^{jT(q)} \qquad \text{as} \quad j \to -\infty \,.$$

A standard linear regression can be used to estimate the partition function $T(q)$ since the values $E|d_{j,k}|^q$ could be easily obtained by the moment-matching method.

Let $\widehat{S_j(q)} = \frac{1}{2^j} \sum_{k=1}^{N2^{-j}} |d_{j,k}|^q$ be the empirical q^{th} moment of the wavelet coefficients (N is the length of the time series). By applying the Central Limit Theorem, $\widehat{S}_j(q) \to E|d_{j,k}|^q$ as $N \to \infty$. Then, using the scaling property of the wavelet coefficients given by $d_{j,k} = 2^{jH} d_{0,k}$, we have that $\widehat{S}_j(q)$ is asymptotically normal with mean $2^{jT(q)} E|d_{0,0}|^q$ and variance $\sigma_{j,q}^2 = \frac{2^{2jT(q)} \operatorname{Var}|d_{0,0}|^q}{2^{-j}N}$ (see, [11]). Considering the logarithm transformation of $\widehat{S_j(q)}$ we can write

$$(4.5) \qquad \log_2 \widehat{S_j(q)} = j\,T(q) + \varepsilon_j \,,$$

where the error term ε_j is introduced from the moment matching method when replacing the true moments with the empirical ones. Using approximation theorems (see, [26]) one can prove that the $\log_2 \widehat{S_j(q)}$ is asymptotical normal with

mean and variance described by [11]. The ordinary least square (OLS) estimator gives the estimation of the partition function,

$$(4.6) \qquad \widehat{T}(q) := \sum_{j=j_1}^{j_2} a_j \log_2 \widehat{S}_j(q) ,$$

where the regression weights a_j must verify the two conditions $\sum_j a_j = 0$ and $\sum_j j\, a_j = 1$ (see [2] and [5]). Thus, we can estimate $f(\alpha)$ through a local slope of $\widehat{T}(q)$ at values

$$\widehat{\alpha}(q_l) = \left[\widehat{T}(q_{l+1}) - \widehat{T}(q_l)\right]/q_0 , \qquad q_l = l\,q_0 ,$$

as

$$\widehat{f}\big(\alpha(q_l)\big) = q_l\,\alpha(q_l) - \widehat{T}(q_l) .$$

Multifractal spectra can even be found for monofractal processes, where the spectra generated from such processes are ramp-like with a dominant (modal) irregularity corresponding to the theoretical Hurst exponent (see [23]). The MFS can be easily generalized to higher dimensions (see [6, 22]).

4.1. Multifractal descriptors

The multifractal spectrum can be approximately described by three canonical descriptors, which are:

(**1**) Spectral Mode (Hurst exponent, SM);

(**2**) left slope (LS) or left tangent (LT);

(**3**) width spread (Broadness, B) or right slope (LS) or right tangent (RT).

A typical multifractal spectrum can be quantitatively described as shown in Figure 7. In particular, SM represents the apex of spectrum or most common Hölder regularity index α found within the signal, and LS (or LT) represents the slope of the distribution produced by the collection of Hölder regularity index α with smaller values of the mode (SM). However, broadness (B) is a more intricate descriptor of the multifractal spectrum. Broadness (B) is believed to be more meaningful than right slope (RS) or right tangent (RT), because it is a compound measure representing the overall nature of the multifractal spectra, taking into account the overall variability among the Hölder regularity index α. In addition, broadness (B) partially accounts for right slope (RS) or right tangent (RT) in calculation, as the resulting value of B is based on the relative values of RS and LS. Both slopes (or both tangents) can be easily obtained using the interpolation technique, while it is not straightforward to define the broadness (B) automatically. There are many ways to define the broadness (B). In this work, we select the method proposed by [27]. The overall multifractal descriptors are also graphically presented in Figure 7.
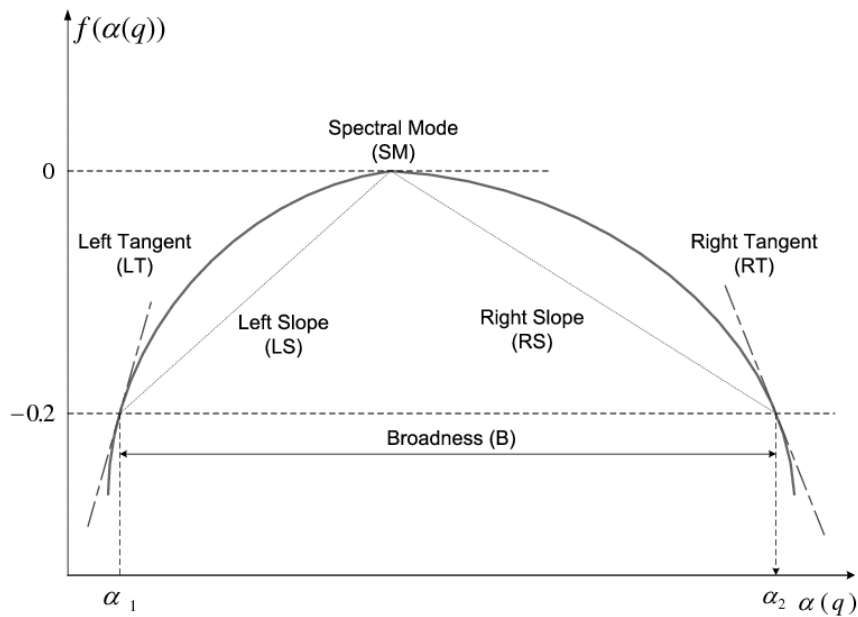
Figure 7: Illustration of geometric descriptors of multifractal spectra. Note that the horizontal axis represents values of Hölder regularity index $\alpha(q)$, while the vertical axis represents values proportional to the relative frequency of these indices, $f(\alpha(q))$.

4.2. Application to mammographic tissue images

In this section, we apply the wavelet-based multifractal spectra to two digital mammogram images (shown in Figure 8) of size 512×512 representing mastopathic and cancerous tissues. We refer to the paper of [12] for a detailed description of the images.
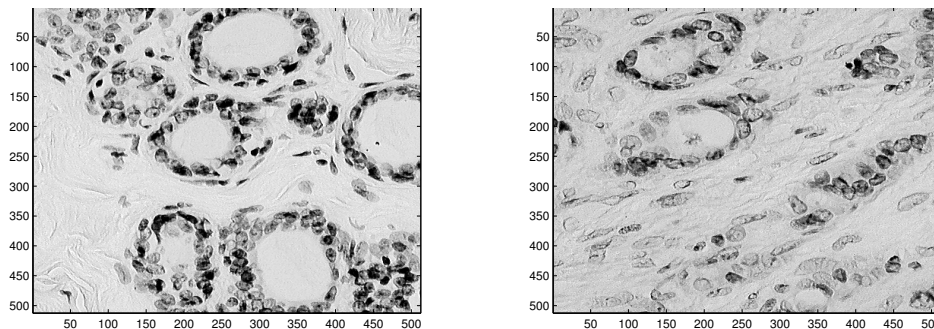

Figure 8: (a) Mastopathic tissue;
(b) Mammary cancer (invasive ductal mammary carcinoma).

First, we perform the 2D discrete complex wavelet transform for each image of size 512×512 by using complex Daubechies 6-tap filter (see [12, 15]), then we evaluate the wavelet multifractal spectra by extending (4.1) and (4.3) to 2D. Figure 9 compares the multifractal spectrum of the mastopathic tissue with the cancerous mammogram image. Although they seem to have a similar behavior it is evident that the Hurst exponents representing the local regularity are different for the two images.
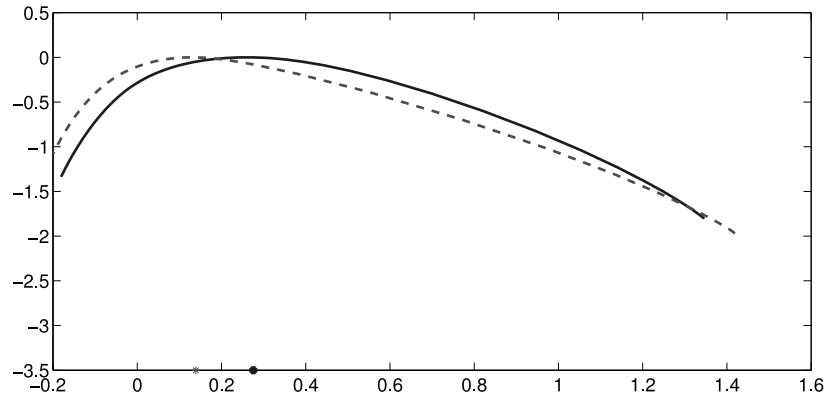

Figure 9: Wavelet multifractal spectrum for the mastopathic tissue (solid line) and cancerous tissue (dashed line). The filled dot and the asterisk on the horizontal axis represent the spectral mode for the mastopathic and cancerous tissue, respectively.

The different fractality is also confirmed by the calculation of the multi-fractal descriptors shown in Table 3. The mastopathic tissue seems to be more regular than the cancerous one (the regularity is represented by the SM or Hurst exponent) and the range (or broadness) of the local Hölder index is larger than for the cancerous tissue.

Table 3: Wavelet multifractal descriptors.

Tissue	H	L1	L2	R1	R2	B
masto	0.26	2.2	-1.2	0.89	-0.70	0.51
mamca	0.13	2.8	-1.2	1.15	-0.76	0.43

Hence, we conclude that the multifractal spectrum and its descriptors could be used in classification algorithms for discriminating between mastopathic and cancerous tissue. This could provide an automatic tool to support medical decisions.

5.   DISCUSSION AND CONCLUSION

Due to its prevalence and mortality a cancer diagnosis is one of the main fears of the general public. Certainly due to modern diagnostic tools as well as improvements in therapy, cancer can be seen as a chronic disease, where some of the patients will be living for several years after diagnosis. Earlier studies have proven that a positive attitude will lead to a significant increase in life expectancy of cancer patients. The risk of suicide or a burn-out is rapidly increasing within the first weeks after cancer diagnosis due to the very stressful first period. Utilizing psycho-oncologic care gives assistance in these situations. However, this option is quite unknown to most patients such that only 1% uses this support [25]. All these facts support the necessity to find quick, semi or full-automated methods for tissue discrimination. The discrimination between the groups in terms of distributional fit allows the interpretation that more abnormal tissue follows normal distribution. Moreover, it has been shown that gamma as well as Weibull distributions are proper distributions for fitting mammary as well as mastopathic box-counting dimensions. Combining several instruments for cancer testing is of major importance, because e.g. deciding for mammary cancer or mastopathy just on the basis of box-counting dimension may lead to many miss-specifications. Medical staff can be supported in the decision process by these fractal measures, nevertheless, other supporting tools as shape analysis of the cancer (see [14] among others) or alternative cancer therapies in cases of high risks for cancer (see [25]) are desired to have the highest possible medical attendance for patients. Additionally the impact of environmental factors on developing cancer or as preventive strategy have to be taken into account.

Criticism on the use of screening mammography due to over-diagnosis led some researchers to show that one in three breast cancers identified by mammography would not cause symptoms in a patient's lifetime (see [16]). Therefore, alternative and accurate screening technologies must be developed. The functional and technical background of dynamic infrared (IR) imaging has the potential for early detection of breast cancer and treatment response evaluation if optimal diagnostic algorithms are developed. We have shown that the wavelet-based multifractal analysis of dynamic IR thermograms is able to discriminate between cancerous breasts with monofractal (cumulative) temperature temporal fluctuations characterized by a unique singularity exponent ($h = c_1$), and healthy breasts with multifractal temperature fluctuations requiring a wide range of singularity exponents as quantified by the intermittency coefficient $c_2 \gg 0$.

ACKNOWLEDGMENTS

REFERENCES

[1] ABRÀMOFF, M.D.; MAGALHÃES, P.J. and RAM, S.J. (2004). Image processing with ImageJ, *Biophotonics international*, **11**(7), 36–43.

[2] ABRY, P.; ROUX, S.; VEDEL, B. and WENDT, H. (2010). *The contribution of wavelets in multifractal analysis.* In "Wavelet Methods in Mathematical Analysis and Engineering, Series in contemporary applied mathematics" (A. Damlamian and S. Jaffard, Eds.), 55–98.

[3] BAISH, J.W. and JAIN, R.K. (2000). Fractals and cancer, *Cancer Res.*, **60**, 3683–3688.

[4] CHEN, D.R. *et al.* (2005). Classification of breast ultrasound images using fractal feature, *Clinical Imaging*, **29**(4), 235–245.

[5] DELBEKE, L. and ABRY, P. (2000). Stochastic integral representation and properties of the wavelet coefficients of linear fractional stable motion, *Stochastic Processes and their Applications*, **86**, 177–182.

[6] DERADO, G.; LEE, K.; NICOLIS, O.; BOWMAN, F.D.; NEWELL, M.; RUGGERI F. and VIDAKOVIC, B. (2008). *Wavelet-based 3-D Multifractal Spectrum with Applications in Breast MRI Images.* In "Bioinformatics Research and Applications" (Mandoiu, Sunderraman and Zelikovsky, Eds.), Lecture Notes in Computer Science, Springer, 281–292.

[7] DOUBENI, C.A. *et al.* (2012). Contribution of Behavioral Risk Factors and Obesity to Socioeconomic Differences in Colorectal Cancer Incidence, *JNCI – J. Natl. Cancer Inst.*, **104**(18), 1353–1362.

[8] ELLIS, R.S. (1984). Large Deviations for a General Class of Random Vectors, *The Annals of Probability*, **12**(1), 1–12.

[9] FRISCH, U. and PARISI, G. (1985). *On the singularity structure of fully developed turbulence.* In "Turbulence and Predictability in Geophysical Fluid Dynamics and Climate Dynamics" (M. Gil, R. Benzi and G. Parisi, Eds.), 84–88, Amsterdam, North-Holland, Elsevier.

[10] GEORGE, L.E. and KAMAL, H.S. (2007). *Breast cancer diagnosis using multifractal dimension spectra.* In "2007 IEEE International Conference on Signal Processing and Communications (ICSPC 2007)".

[11] GONÇALVES, P.; RIEDI, H. and BARANIUK, R. (1998). *Simple statistical analysis of wavelet-based multifractal spectrum estimation.* In "Proceedings 32nd Asilomar Conference on Signals, Systems and Computers", Pacific Grove, CA, Nov. 1998.

[12] HERMANN, P.; MRKVIČKA, T.; MATTFELDT, T.; MINÁROVÁ, M.; HELISOVÁ, K.; NICOLIS, O.; WARTNER, F. and STEHLÍK, M. (2015). Fractal and stochastic geometry inference for breast cancer: a case study with random fractal models and Quermass-interaction process, *Statistics in Medicine*, **34**(18), 2636–2661. doi:10.1002/sim.6497

[13] HERMANN, P.; PIZA, S.; RUDERSTORFER, S.; SPREITZER-GRÖBNER, S. and STEHLÍK, M. (2014). Fractal Case Study for Mammary Cancer, *Biometrie und Medizinische Informatik – Greifswalder Seminarberichte*, **23**, 149–166.

[14] HERMANN, P. and STEHLÍK, M. (2015). *On some issues on statistical analysis for Wilms tumor.* In "Proceedings of the 30th International Workshop on Statistical Modelling" (H. Friedl and H. Wagner, Eds.), Volume 2, Springer, 115–118.

[15] JEON, S.; NICOLIS, O. and VIDAKOVIC, B. (2014). Mammogram diagnostics via 2-D complex wavelet based self-similarity measures, *The São Paulo Journal of Mathematical Sciences*, **8**(2), 265–284.

[16] JØRGENSEN, K.J. and GØTZSCHE, P.C. (2009). Overdiagnosis in publicly organised mammography screening programmes: systematic review of incidence trends, *BMJ Publishing Group Ltd*, **339**, b2587.

[17] MANDELBROT, B. (1969). Long-run linearity, locally Gaussian process, H-spectra, and infinite variances, *International Economic Review*, **10**, 82–111.

[18] MANDELBROT, B. (1972). A statistical methodology for non-periodic cycles: From the covariance to R/S analysis, *Annals of Economic and Social Measurement*, **1**, 259–290.

[19] MRKVIČKA, T. and MATTFELDT, T. (2011). Testing histological images of mammary tissues on compatibility with the boolean model of random sets, *Image Anal. Stereol.*, **30**, 11–18.

[20] PASEKA, J.; SOLOVYOV, S.A. and STEHLÍK, M. (2015). Lattice-valued bornological systems, *Fuzzy Sets and Systems*, **259**(15), 68–88.

[21] PASEKA, J.; SOLOVYOV, S.A. and STEHLÍK, M. (2014). On the category of lattice-valued bornological vector spaces, *Journal of Mathematical Analysis and Applications*, **419**, 138–155.

[22] RAMÍREZ-COBO, P. and VIDAKOVIC, B. (2013). A 2D wavelet-based multiscale approach with applications to the analysis of digital mammograms, *Computational Statistics & Data Analysis*, **58**, 71–81.

[23] RIEDI, R.H. (1999). Multifractal Processes, *Technical Report* 99-06.

[24] RIEDI, R.H. (1998). *Multifractals and Wavelets: A potential tool in Geophysics.* In "Proceedings of the SEG Meeting", New Orleans, Louisiana/USA.

[25] RUNOW, K.D. (2013). *Krebs – Eine Umweltkrankheit? Risiko minimieren, Therapie optimieren*, Südwest Verlag, München.

[26] SERFLING, R. (1980). *Approximation Theorems of Mathematical Statistics*, Wiley.

[27] SHI, B.; MOLONEY, K.P.; PAN, Y.; LEONARD, V.K.; VIDAKOVIC, B.; JACKO, J.A. and SAINFORT, F. (2006). Wavelet classification of high frequency pupillary responses, *Journal of Statistical Computation and Simulation*, **76**(5), 431–445.

[28] STEHLÍK, M. (2016). On convergence of topological aggregation functions, *Fuzzy Sets and Systems*, **287**, 48–56.